IEEE Access
Multidisciplinary | Rapid Review | Open Access Journal

Received April 28, 2022, accepted May 11, 2022, date of publication May 16, 2022, date of current version May 19, 2022.

Digital Object Identifier 10.1109/ACCESS.2022.3175161

A Novel Reflection-Type Polarization Convertor Design Using Connected Orthogonal Tightly Coupled Dipole Arrays

SEONGJUNG KIM, (Student Member, IEEE), AND SANGWOOK NAM, (Senior Member, IEEE)
School of Electrical and Computer Engineering, Institute of New Media Communication (INMC), Seoul National University, Seoul 08826, South Korea

Corresponding author: Sangwook Nam (snam@snu.ac.kr)

This work was supported in part by the Institute of Information and Communications Technology Planning and Evaluation (IITP) Grant through the Korea Government (MSIT), Millimeter-Wave Metasurface-Based Dual-Band Beamforming Antenna-on-Package Technology for 5G Smartphone, under Grant 2020-0-00858; and in part by the BK21 FOUR Program of the Education and Research Program for Future ICT Pioneers, Seoul National University, in 2021.

ABSTRACT Herein, we design a polarization convertor (PC) using two orthogonally polarized, tightly coupled dipole arrays (TCDAs) connected in cascade, of which one is used for the reception of incident waves and the other is used for their transmission. The operation of the PC is elucidated via a cascading equivalent circuit of unit cells of orthogonally polarized TCDAs. The critical role of vertical metal strips (VMSs) with regard to wide-angle insensitivity is discussed. Moreover, it is found that the undesirable common mode occurs under oblique incidence and its frequency is related to the size-to-height ratio of the unit cell. To demonstrate the performance of the proposed PC, a 40 $\times$ 40 array structure is fabricated and measured using the Naval Research Laboratory (NRL) arch method. The simulated bandwidth range is 2.06 to 14.54 GHz (7.06:1) for a polarization conversion ratio (PCR) $\geq$ 80%, and the measured bandwidth range is 1.68 to 14.51 GHz (8.64:1) for a PCR $\geq$ 72% at an incident angle of 10°. At an incident angle of 40°, the simulated and measured bandwidths are 2.15 to 14.13 GHz (6.57:1) and 2.43 to 13.87 GHz (5.71:1) for a PCR $\geq$ 80%, respectively.

INDEX TERMS Reflection-type polarization convertor, ultra-wideband, tightly coupled dipole array.

I. INTRODUCTION

The demand for polarization control has expanded to include the manipulation of electromagnetic wave propagation [1]. Such manipulation can be broadly divided into two categories, namely reflection [2], [3] and transmission [4], [5], according to the direction of the outgoing wave. Polarization state conversion can also be classified as linear-to-linear, circular-to-linear, or circular-to-circular [6]–[8]. This study focuses on reflection-type polarization convertors (PCs) with linear-to-linear conversion. PCs can be used in several applications, such as in the reduction of spatial field mutual coupling [9], reduction of scattering cross-sections (SCSs) [10], and widening of the impedance bandwidth of antennas [11], [26]. When designing PCs, the main factors to be considered are the bandwidth, thickness, and incident angle sensitivity. Typically, if wide-angle insensitivity or ultra-thin properties are attained, then the bandwidth is strictly narrow, and vice versa [12]–[16]. Numerous PCs are ultra-thin and have fundamentally limited bandwidths owing to their resonant-type structure. The operating principle of a resonant-type structure is to make the phase difference of two orthogonally polarized reflected waves be equal to 90°, as well as to ensure that the polarization of the reflected wave is orthogonally rotated.

In this paper, a novel approach is proposed to design a PC. A tightly coupled dipole array (TCDA) can be a non-resonant-type PC. It was introduced by Volakis and Sertel in 2011 [17]. They utilized TCDAs to reduce the velocity of waves laterally traveling along the structure and achieved smaller radiofrequency (RF) structures. As a result, TCDAs can provide ultra-wideband capabilities when large arrays are employed. Subsequently, many papers on TCDA antennas have been published [18]–[27]. According to the reciprocity theorem, a wideband transmitting antenna can function as a wideband reception antenna. Therefore, several studies

The associate editor coordinating the review of this manuscript and approving it for publication was Tutku Karacolak.

have applied TCDAs in applications such as phase modulated reflect arrays [28], [29], transmit arrays [30], and absorbers [31], [32]. As an extension of the concept of TCDAs as ultra-wideband and wide-angle transmission and reception arrays, we propose the use of two orthogonally polarized TCDAs connected in cascade for the design of PCs. Here, a vertically polarized TCDA is connected to a horizontally polarized TCDA, wherein one TCDA is used for the reception of incident waves and the other functions as a transmission array corresponding to the orthogonal polarization direction. Numerous resonant- or non-resonant-type antenna arrays have been developed over the past decades. Therefore, it should be noted that by using the proposed approach, almost all antennas array can be utilized for developing PCs, including resonant-type antenna arrays such as patch-antenna arrays.

The remainder of this paper is organized as follows: the design procedure of the wideband TCDA unit cell antenna and the wideband TCDA-based PC unit cell is presented. The operating principles of the TCDA antenna and PC are slightly different. Therefore, the equivalent circuits for the unit cells of the TCDA antenna and TCDA-based PC are presented and compared. The vertical metal strip (VMS) [22], [33] plays a significant role in making the PC wide-angle insensitive. Therefore, this concept is explained in detail. The results of this study are then compared with those of existing state-of-the-art studies. Important design constraints required to eliminate the common mode resonant frequency from the target band are considered. The experimental results obtained using horn antennas are discussed next. Finally, the conclusions of the study are summarized.

II. BRIEF DESCRIPTION OF THE TCDA ANTENNA OPERATION PRINCIPLES

TCDA antennas are widely used for their low-profile, wideband, and wide-angle-insensitive characteristics. Figure 1 shows the proposed unit cell of a TCDA antenna. The four side boundaries represent the unit cell boundary conditions, and the top surface is terminated by the Floquet port (FP). The dielectric superstrate reduces the Floquet air impedance and changes the responses for oblique incident or radiating waves [21], [34], [35]. Based on a previous TCDA structure [21] and a cylindrical VMS structure [22], [33], the optimized geometrical parameters of the unit cell to achieve the best performance were determined as follows: $A = 8$ mm, $C = 5.19$ mm, $D = 1$ mm, $H = 9$ mm, $a = 6$ mm, $b = 0.59$ mm, $c = 0.2$ mm, $d = 1.41$ mm, $e = 0.5$ mm, $f = 0.65$ mm, $g = 0.1$ mm, $h = 0.12$ mm, $i = 0.17$ mm, $j = 0.75$ mm, $k = 0.28$ mm, $l = 0.18$ mm, and $m = 0.1$ mm. Figure 1(c) shows an equivalent circuit of the TCDA antenna [22]. For the dominant radiating Floquet modes, the wave numbers are as follows:

$$k_{z00}^{+} = \sqrt{\varepsilon_r} k_0 \cos\theta, \quad k_{z00}^{-} = k_0 \cos\theta \tag{1}$$

where ε_r is relative dielectric constant of the superstrate, k_0 is the wave number in free space, and θ is the propagation

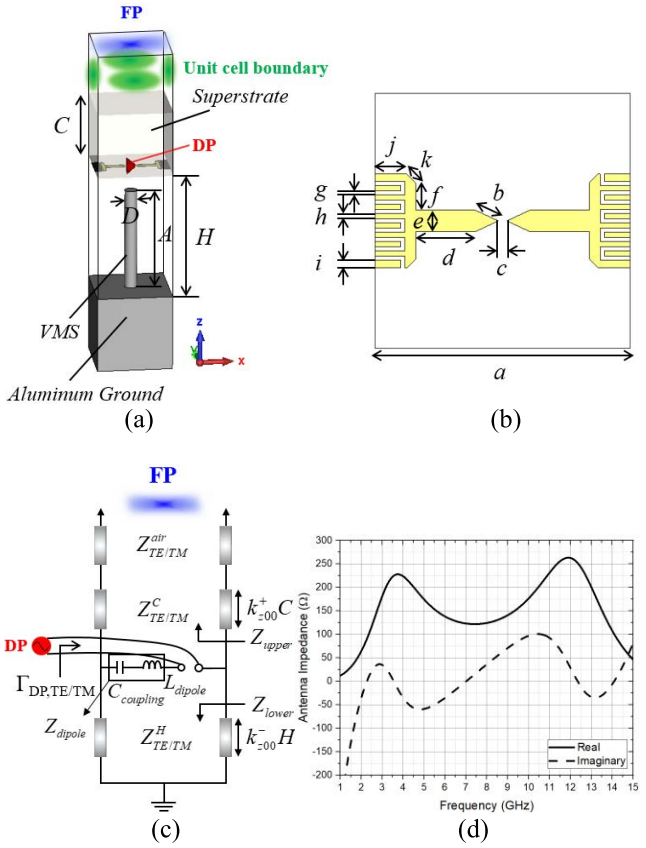

FIGURE 1. Unit cell structure of the single-polarized TCDA antenna used to design the proposed PC. (a) Schematic diagram of the structure. The height of the space between the superstrate and ground is H, and the length of the VMS is A; $H > A$ as the VMS is not in contact with the superstrate. The superstrate is Taconic RF-30 ($\varepsilon_r = 3$, $tan\delta = 0.0019$). (b) Bottom-side metallic pattern of the superstrate with unit cell size $a \times a$. The discrete port (DP) is located at the space with length c between the side arms. (c) Equivalent circuit of the TCDA antenna where the H-A (= 1 mm) region is ignored to simplify the model. (d) Antenna impedance at the DP for broadside radiation.

angle from the +z-axis. The characteristic impedance of the transmission lines can be expressed as follows:

$$Z_{TE} = \eta_0 \sqrt{\frac{\mu_r}{\varepsilon_r}} \frac{d_x}{d_y} \frac{1}{\cos\theta}, \quad Z_{TM} = \eta_0 \sqrt{\frac{\mu_r}{\varepsilon_r}} \frac{d_x}{d_y} \cos\theta \tag{2}$$

where η_0 is the characteristic impedance in free space (377 Ω), μ_r is the relative permeability (in this case it is equal to 1), and ε_r is 1, except for the case of $Z_{TE/TM}^{C}$. Here, *TE/TM* indicates the transverse electric/magnetic field mode. For the TCDA unit cell structure, the TE and TM modes are excited when scanning along the y- and x-axes, respectively. In the other directions, both modes are simultaneously excited. d_x and d_y are lengths of the unit cell along the x- and y-axis, respectively (in this case, the ratio of these values is 1). $\Gamma_{DP,TE/TM}$ is the reflection coefficient of the TE and TM modes at the DP, which is expressed as $\Gamma_{DP,TE/TM} = (Z_{ant} - Z_{port})/(Z_{ant} + Z_{port})$ where Z_{ant} and Z_{port} are the antenna impedance and internal impedance of the DP, respectively. Z_{ant} is plotted in Fig. 1(d), and Z_{port} was set to 150 Ω in

this study, which is the average real value of the antenna impedance utilized to minimize reflection.

The interdigital capacitance increases the series capacitance ($C_{coupling}$) and partially cancels out the shunt inductance from the downward transmission line with a length of $k_{z00}^{-}H$ terminated by the aluminum ground at low-frequency bands. Furthermore, at high-frequency bands, the self-inductance of the dipole (L_{dipole}) partially cancels out the shunt capacitance from the transmission line. Finally, this results in a wideband operation. Z_{ant} can be expressed as $Z_{ant} = Z_{dipole} + Z_{upper}//Z_{lower}$. At low-frequency bands, Z_{lower} is the dominant factor of Z_{ant}. In particular, this parameter is significant when scanning the beam and the TM mode is dominantly excited because k_{z00}^{-} and Z_{TM}^{H} simultaneously decrease. That is, Z_{lower} and Z_{ant} rapidly become a small value that can be determined using the following equation (3) [22]:

$$Z_{lower} = jZ_{TE/TM}^{H} \tan(k_{z00}^{-}H). \tag{3}$$

For the TM mode, the VMS can alleviate this rapid behavior by making k_{z00}^{-} and $Z_{TE/TM}^{H}$ to be k_0 and Z_{TEM}^{H}, respectively, where Z_{TEM}^{H} is 377 Ω. Therefore, Z_{lower} is independent of θ and may be expressed as Equation (4) [22], [33]:

$$Z_{lower} = jZ_{TEM}^{H} \tan(k_0 H). \tag{4}$$

As a result, the TCDA with a VMS can be wide-angle insensitive. It is worth noting that the reflections at the surface of the VMS region $(Z_{TEM}^{H}-Z_{TM}^{H})/(Z_{TEM}^{H}+Z_{TM}^{H})$ are < -10 dB up to $\theta = 60°$. Conversely, for the TE mode, Z_{lower} does not exhibit rapid behavior because Z_{TE}^{H} increases while k_{z00}^{-} decreases. In general, the bandwidth of TCDA antennas is >5:1, and the thickness is ∼0.1 λ_{low} at the lowest operating frequency [18]–[27]. Moreover, the response is well-preserved up to a scanning angle of 45°.

III. DESIGN AND OPERATION PRINCIPLES OF THE TCDA-BASED PC

The design of a PC using a conventional TCDA is simple as the transformation is achieved by combining two linear TCDAs orthogonal to each other such that each dipole arm is connected to an orthogonal dipole arm. The proposed PC using the TCDA structure (Fig. 1(a)) is shown in Fig. 2. Based on the reciprocity theorem, wideband transmitting antennas can function as wideband receiving antennas. The TCDA dipole with polarization matched to that of an incident wave acts as a wideband receiving antenna, and the orthogonal dipole connected to it works as a wideband transmitting antenna with polarization orthogonal to that of the incident wave. All dimensions of the structure are same as in Fig. 1, except for the connecting lines *m* and *l*.

Figure 3(a) schematically presents the operating principle of the proposed PC. When the y-polarized wave impinges on the PC, the y-polarized TCDA acts as a receiving array such that a surface current J_{ind} is induced along the same direction as the incident polarization, and the induced current flows

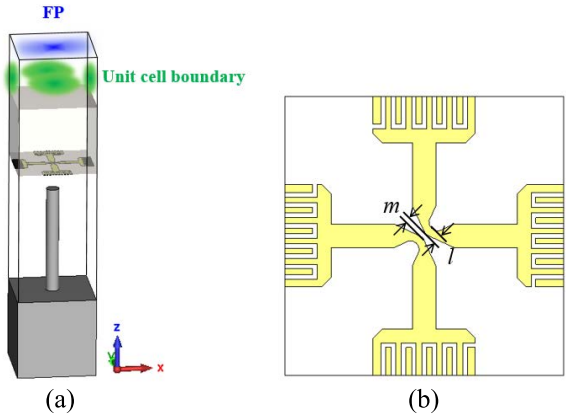

FIGURE 2. Proposed unit cell structure of the dual-polarized PC; the patterns are based on the TCDA (Fig. 1a). (a) Overall view of the structure. (b) Bottom-side of the superstrate. Each arm of the vertical (horizontal) TCDA dipoles is connected to the corresponding orthogonal dipole arm by a connecting line of width *l*.

along the orthogonal dipole arm. As a result, the x-polarized TCDA now acts as a transmitting array and generates the x-polarized reflected wave. It should be noted that the orthogonal current is induced only when two orthogonal dipoles (i.e., two TCDA antennas) are impedance-matched. In the impedance-matched band (in this case, 1.98 to 14.59 GHz), the induced current flows along the orthogonal dipole arm, as shown in Fig. 3(b).

The operation principle of this system can be explained based on the incident and scattered fields, as shown in Fig. 4. It is important to note that although the J_x and J_y surface currents are simultaneously induced, the net radiating field component only corresponds to J_x when the y-polarized wave is irradiated. Considering the operation principle of the TCDA, the *b* and *c* or *d* and *e* fields are in phase at the operating frequency band [17]. Moreover, the *c* and *e* fields involve multiple reflection effects between the TCDA surface and the aluminum ground. Due to the boundary condition of the TCDA copper surface, the direction of induced current is the same as that of incident electric field and opposite to that of the scattered electric field. As a result, the *a*(+z traveling), *b*, and *c* fields cancel out one another, and only the *d* and *e* fields radiate in the z-direction, which is referred to as the polarization conversion principle. However, it should be noted that outside of the operating band, J_x and J_y are not induced. Therefore, *a*, *b*, and *c* do not cancel one another out.

In Fig. 5, the operation principle of the PC can also be interpreted by comparing the equivalent circuits of the TCDA antenna and dual-polarized PC. For the TCDA antenna, the impedance matching at the DP can be achieved when $\Gamma_{DP,TE/TM} \approx 0$ ($Z_{ant} \approx Z_{port}$). Conversely, for the PC, impedance matching of the reflection coefficients r_{yy} (y- to y-polarization) at the FP can be achieved when $\Gamma_{DP,TE/TM} \approx (\Gamma_{DP,TM/TE})*$ because the networks of the TCDA (TE and TM modes) are passive and nearly lossless [36], wherein

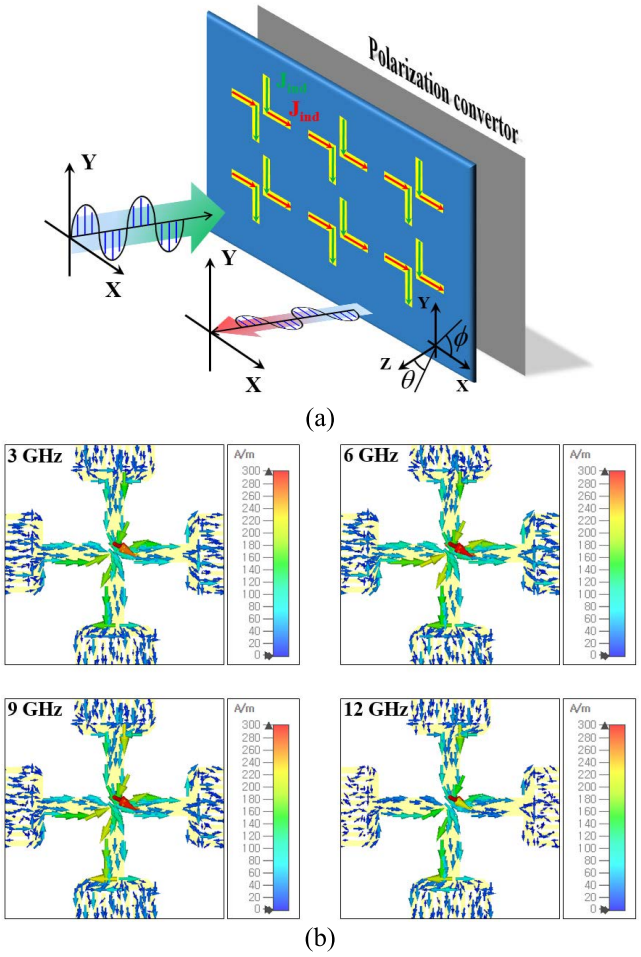

FIGURE 3. Schematic representation of the operating principle of the proposed PC. (a) Operating concept (the superstrate is hidden); the y-polarized incident wave is scattered and converted to an x-polarized reflected wave by the induced current on the PC. (b) Induced current on the PC unit element at various frequencies.

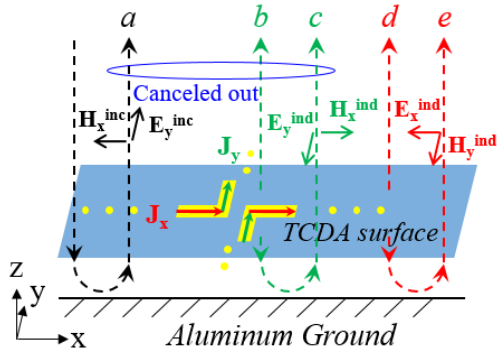

FIGURE 4. Schematic of the incident and scattered fields wherein the superstrate is hidden.

the internal impedance of the FP is $Z^{air}_{TE/TM}$. Moreover, the amplitudes of r_{yy} and r_{xx} are nearly equivalent. We therefore focused only on r_{yy} in this study. Thus, it is important to design a wideband PC wherein the real and imaginary components of $\Gamma_{DP,TE/TM}$ are not extreme values. Conventional

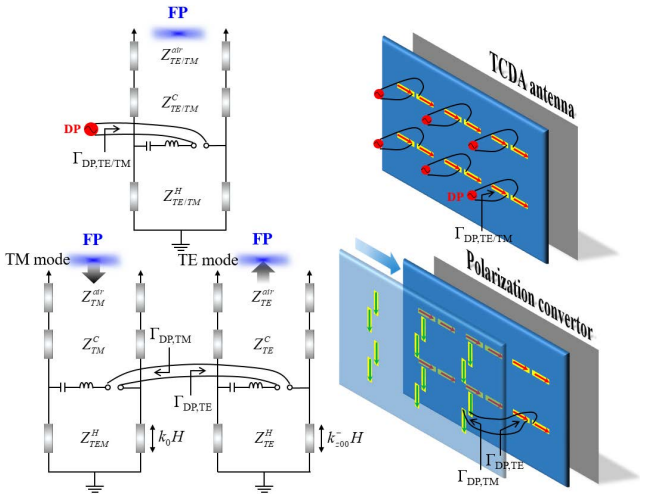

FIGURE 5. Equivalent circuits for the single-polarized TCDA antenna (top) and dual-polarized PC (bottom). For the circuit of the PC, the incident wave is assumed via the TM mode. The parasitic effects corresponding to the connecting line with gap *m* and width *l* in Fig. 2(b) are ignored because the result is almost unchanged by these effects. Here, the superstrate is hidden.

TCDAs satisfy this condition in general [18]–[27]. The equivalent circuit of the PC includes the equivalent circuits of the TE and TM modes of the TCDA in cascade because the TM mode that is obliquely incident to the PC is converted to the TE mode in the specular direction, and vice versa. Owing to the VMS, the VMS region of the equivalent circuit for the TM mode differs from that of the TE mode.

In Fig. 6, the real and imaginary values of the reflection coefficient $\Gamma_{DP,TE/TM}$ at the DP are not large owing to the operation principle of the TCDA [18]–[27], which results in a wideband PC. In the frequency range satisfying $\Gamma_{DP,TE/TM} \approx (\Gamma_{DP,TM/TE})*$, the real components have similar values, the imaginary components are sufficiently small or exhibit opposite signs, and impedance matching at the FP can be achieved. In Fig. 7(a), the reflection coefficients of $\Gamma_{DP,TE}$ are unchanged by the VMS when the beam scans in the H-plane ($\phi = 90°$) exciting the TE mode. In contrast, $\Gamma_{DP,TM}$ is significantly decreased because Equation (4) is constant as a result of the VMSs, as explained in Section II. Interestingly, due to the dual-polarized PC, the reflection coefficients r_{yy} at the FP are simultaneously improved by the VMS even when the incidence angle is changed. This occurs because the equivalent circuits of the TE and TM modes are connected in cascade. Therefore, these two circuits inevitably affect one another. Moreover, considering the VMSs at 2.2 to 5.0 GHz, the condition $\Gamma_{DP,TE} \approx (\Gamma_{DP,TM})*$ is roughly satisfied, as shown in Fig. 7(b). We considered only this frequency range because the difference between the reflection coefficient r_{yy} with and without the VMS is the most significant in this range of the operating band, as shown in Figs. 8(a) and (b). Notably, although $\Gamma_{DP,TE}$ is large when the incident angle is 60°, it is conjugately matched to $\Gamma_{DP,TM}$, as shown in Fig. 7(b), which leads to impedance matching

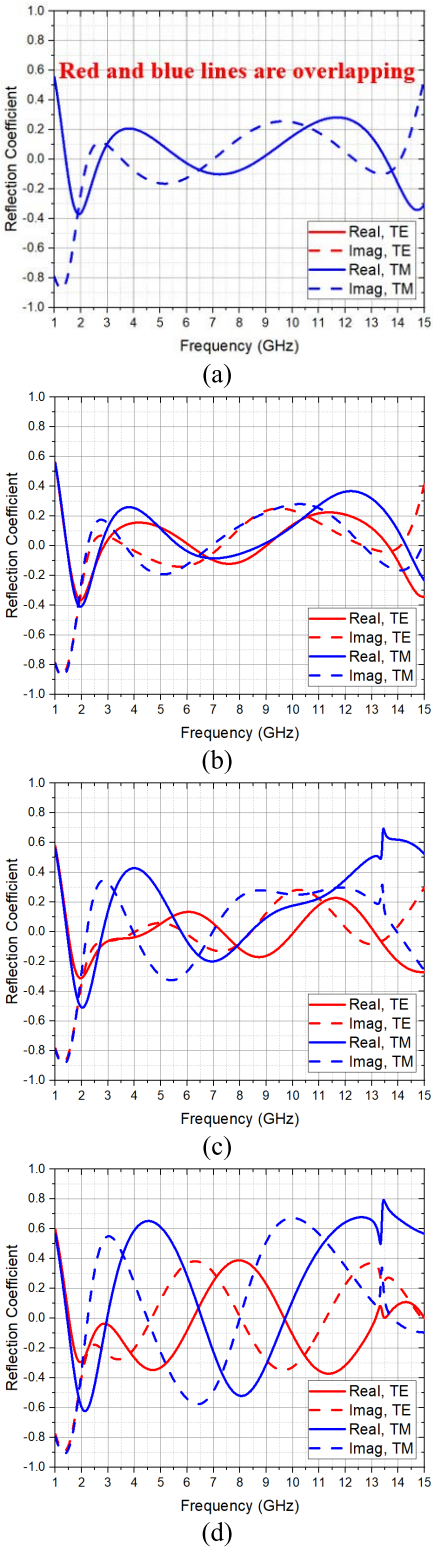

FIGURE 6. Real and imaginary components of the reflection coefficient at the DP of the Fig. 1(a) structure as the beam is scanned along $\phi = 0°$ (TE-mode-excited) and $\phi = 90°$ plane (TM-mode-excited). (a) $\theta = 0°$ (the lines of the TE and TM modes are perfectly overlapped), (b) $\theta = 20°$, (c) $\theta = 40°$, and (d) $\theta = 60°$.

at $r_{yy} \approx 0$. This demonstrates the operation principle of the wide-angle insensitivity of this system. Moreover, the

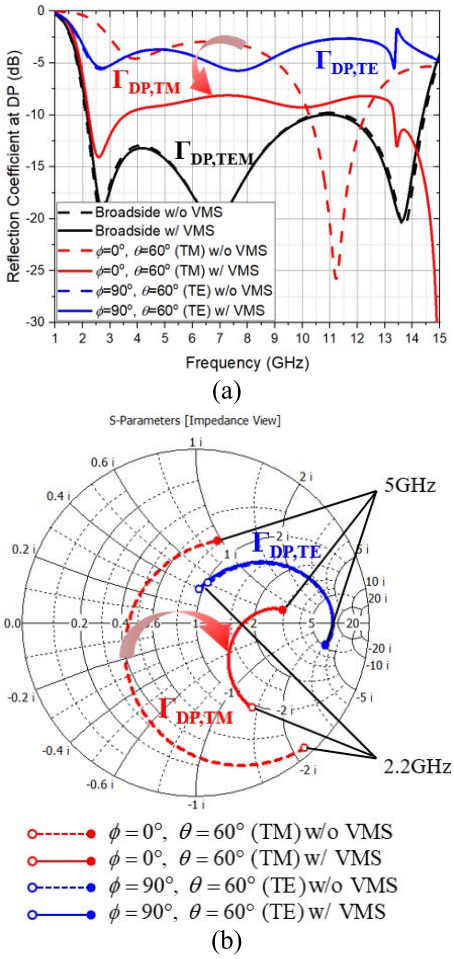

FIGURE 7. (a) Reflection coefficients at the DP of the single-polarized TCDA antenna (Fig. 1(a)) with or without the VMS. When scanning in the plane with $\phi = 0°$ and $\phi = 90°$, the TM and TE modes are excited, respectively. (b) Curves of the reflection coefficients normalized to 50 Ω, which are drawn in the Smith chart for 2.2 to 5 GHz.

transmission coefficient r_{xy} (y- to x-polarization) has the relationship $|r_{xy}|^2 + |r_{yy}|^2 \approx 1$ because the proposed structure is nearly lossless. This indicates that wideband polarization conversion can be realized.

IV. RESULTS AND DISCUSSION

Figure 8 shows the results of a unit cell simulation using r_{xy} and r_{yy} with and without the VMSs for incidence angles in the range of 0° to 60°. Without the VMSs, $\Gamma_{DP,TM}$ becomes large in Fig. 7(b) and r_{xy} is significantly degraded when the PC is obliquely illuminated in Fig. 8(a). However, with the VMSs, $\Gamma_{DP,TM}$ becomes small in Fig. 7(b) and there is little change in r_{xy} up to 60°, as shown in Fig. 8(b). The bandwidth is 1.98 to 14.59 GHz (7.37:1) for $r_{xy} \geq -2$ dB under normal incident illumination, and the corresponding thickness (equivalent to $H + C$) at the lowest operating frequency is 0.09 $\lambda_{1.98GHz}$. For an incidence angle of 60°, the bandwidth is 2.11 to 12.86 GHz (6.09:1) for $r_{xy} \geq -2$ dB, and the corresponding thickness at the lowest operating frequency is 0.1 $\lambda_{2.11GHz}$. Figure 8(c) shows the phase of r_{xy}. Because

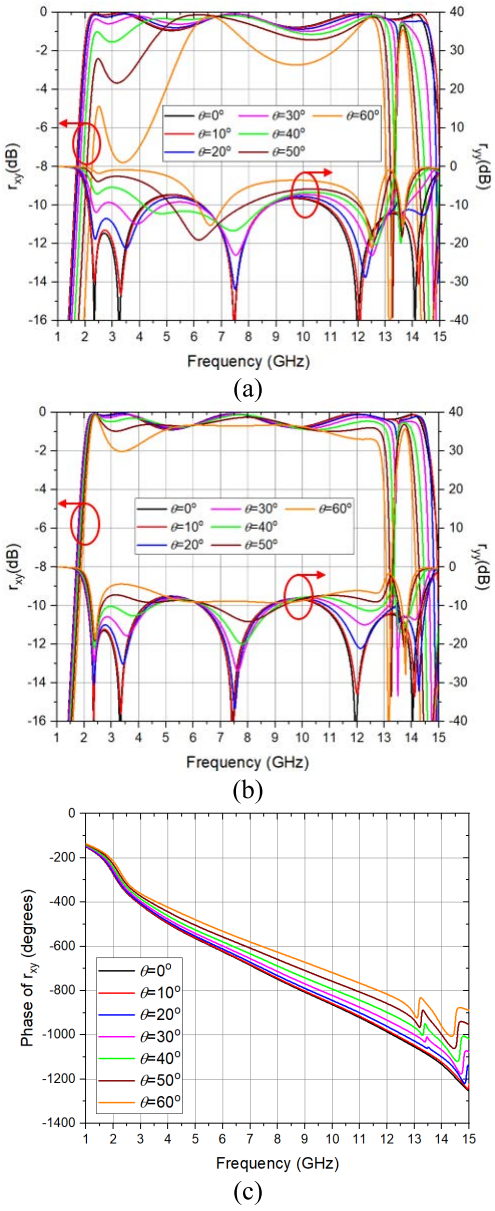

FIGURE 8. Unit cell simulation results for r_{xy} and r_{yy} of the proposed PC (a) without and (b) with the VMS. (c) Phase of r_{xy}.

the proposed PC is not a resonance-type structure like narrow-band PCs, the phase changes progressively and not suddenly.

Table 1 shows a comparison of reflection-type PCs based on the simulated results for a unit cell of the proposed PC and those reported for other state-of-the-art designs. Many previous studies presented results involving r_{xy} at oblique incidence angles without considering the polarization conversion ratio (PCR). Therefore, we present the r_{xy} values to compare the responses of oblique incident waves. The presented PCs [12]–[16] have narrow bandwidths and are insensitive only at small incidence angles, although their thicknesses are small and they possess planar array structures.

TABLE 1. Comparison of unit cell simulation results using reflection-type polarization convertors.

Refs.	r_{xy}	Bandwidth	Thickness	θ
[12]	$r_{xy} \geq -1$ dB	13.08–26.05 GHz (1.99:1)	0.07 $\lambda_{13.08GHz}$	0°
	$r_{xy} \geq -2$ dB	13.44–24.82 GHz (1.85:1)	0.07 $\lambda_{13.44GHz}$	30°
[13]	$r_{xy} \geq -1$ dB	8.49–32.84 GHz (3.87:1)	0.08 $\lambda_{8.49GHz}$	1°
	$r_{xy} \geq -1$ dB	8.71–33.16 GHz (3.81:1)	0.09 $\lambda_{8.71GHz}$	21°
[14]	$r_{xy} \geq -1$ dB	9.73–10.58 GHz (1.09:1)	0.05 $\lambda_{9.73GHz}$	0°
	$r_{xy} \geq -1$ dB	9.68–10.7 GHz (1.11:1)	0.05 $\lambda_{9.68GHz}$	20°
[15]	$r_{xy} \geq -1$ dB	16.26–50.0 GHz (3.08:1)	0.08 $\lambda_{16.26GHz}$	0°
[16]	$r_{xy} \geq -1$ dB	10.09–20.3 GHz (2.01:1)	0.07 $\lambda_{10.09GHz}$	0°
This work	$r_{xy} \geq -1$ dB	2.06–14.45 GHz (7.01:1)	0.1 $\lambda_{2.06GHz}$	0°
	$r_{xy} \geq -1$ dB	2.19–13.89 GHz (6.34:1)	0.1 $\lambda_{2.19GHz}$	50°

To the best of our knowledge, the proposed design has a bandwidth that is considerably wider than that of any other PC and wide-angle insensitivity at the expense of the thickness. In fact, the bandwidth is approximately double that of the PC [13]. In addition, even if the PC is illuminated at 50°, the lowest operating frequency and bandwidth do not change significantly for $r_{xy} \geq -1$ dB. The wide bandwidth observed for normal incident waves is due to the TCDA structure. Moreover, conventional TCDAs have bandwidths of approximately 5:1. However, the bandwidth of the TCDA-based PC can be wider than that of conventional TCDAs because the condition of $Z_{ant} = Z_{port}$ ($Z_{port} = 50\ \Omega$ in general), which limits the band [37], [38], is not required; the matching condition of the PC is only $\Gamma_{DP,TE} \approx (\Gamma_{DP,TM})*$. In addition, the VMSs contribute to the observed wide-angle insensitivity. However, it should be noted that the VMSs can only affect a current sheet array such as TCDAs due to the operation principle of this system [22], and they cannot be applied to parallel-resonance-type PCs [12]–[16]. Therefore, this is a significant advantage of TCDA-based PCs with VMSs, which can uniquely provide a wide bandwidth and exhibit wide-angle insensitivity.

A peculiar phenomenon was observed in the proposed PC array. Even though the structure is symmetric, common mode resonance can be generated when the PC is illuminated at oblique angles, resulting in asymmetric excitation, as shown in Fig. 9(c). The unit cell size a of the TCDA is an important parameter in the design of the TCDA and PC system. In this study, it is found that the unit cell size is related to the common mode generation frequency given the height H, as shown in Fig. 9(b). The proposed length of the unit cells is 6 mm and the height is 9 mm. If the length of the unit cells was 9 mm, then a would equal H and the common mode would be generated at 10.6 GHz with an incidence angle larger than 5°

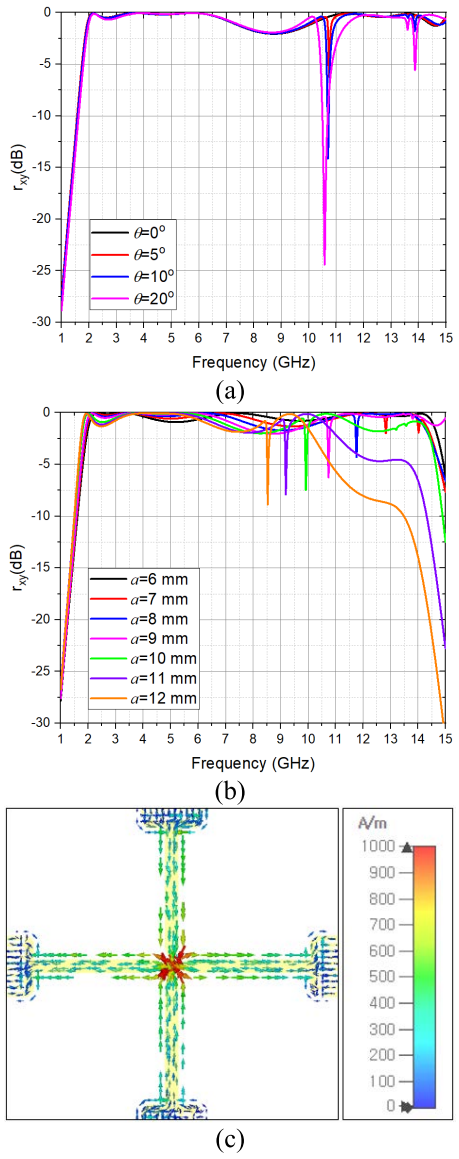

FIGURE 9. Unit cell simulation of r_{xy} of the proposed PC when varying the angle of the incident plane wave or unit cell size. (a) Varying the incidence angle, r_{xy} with $a = 9$ mm. (b) Varying the unit cell size, r_{xy} when the incidence angle θ is 5°. (c) Illuminated at $\theta = 5°$, surface current density of the dipoles with $a = 12$ mm at 8.5 GHz.

in Fig. 9(a). Therefore, even for a sufficiently small incidence angle, an infinite periodic PC array would generate common mode resonance in the operating frequency band. Fig. 9(c) shows the common mode current at 8.5 GHz when the PC unit cell structure with $a = 12$ mm is illuminated at 5°. The common mode current cannot excite a radiating wave effectively, and therefore, the polarization of the incident wave cannot be converted at that frequency and angle. Two observations can be made from Fig. 9(b). First, unit cells with $a \leq 10$ mm do not significantly affect the operating band, except at the common mode frequency. In particular, the lowest operating frequency does not change. Moreover, the height H has a significant effect on the operating band and the lowest operating frequency [32]. Second, the common mode resonant frequency is dependent on a for a given height, where the resonant frequency decreases as the unit cells become larger.

Therefore, to avoid resonance in the band of interest, it is important to select a sufficiently small unit cell size for a given height.

V. EXPERIMENTAL VERIFICATION

Figure 10 shows images of the fabricated 40 × 40 PC array structure. The superstrate comprised two layers of Taconic RF-30 and one layer of adhesive ($\varepsilon_r = 4.3$, $tan\delta = 0.025$). As shown in Fig. 10(a), the edge elements of the array were capacitively coupled to the ground plane via metallic patterns and aluminum spacers, which improved the impedance matching condition [26]. The assembled structure is shown in Fig. 10(b). To avoid any unwanted electromagnetic scattering, plastic bolts were used to tighten the structure through perforated holes in the superstrate. The plastic spacers shown in Fig. 10(c) were used to support the superstrate and maintain the distance between the VMSs and TCDA patterns. The

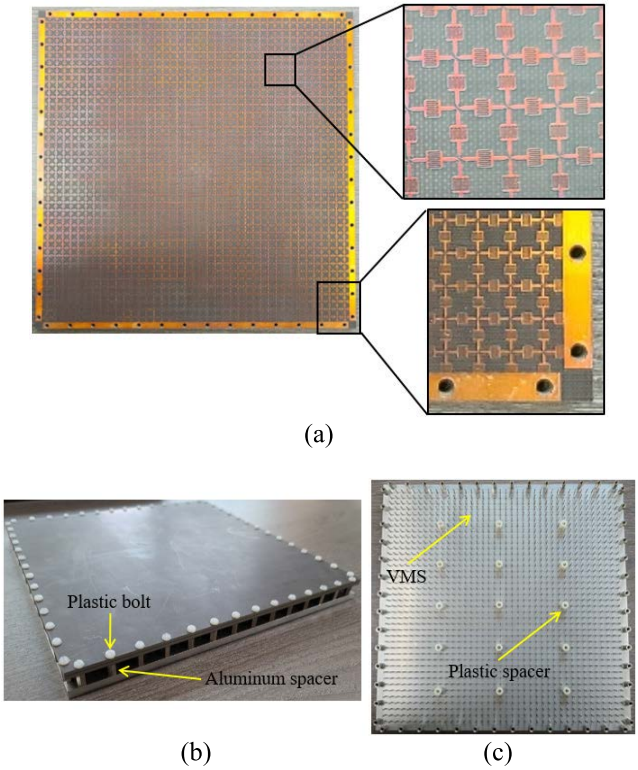

FIGURE 10. Fabricated 40 × 40 PC array structures. (a) Bottom of the superstrate. The edge elements are capacitively coupled to the ground plane via the rectangular edge patterns and aluminum spacers. (b) Overview of the PC. The superstrate is fixed to the aluminum spacers by plastic bolts. (c) The 40 × 40 VMS array with aluminum and plastic spacers is shown without the superstrate. The plastic spacers support the inner space of the superstrate. The plastic spacers have a larger inner diameter than that of the VMSs; the outer diameter of spacers is less than the unit cell size a, and the length of the spacers is equal to H, which is larger than the length of the VMS A.

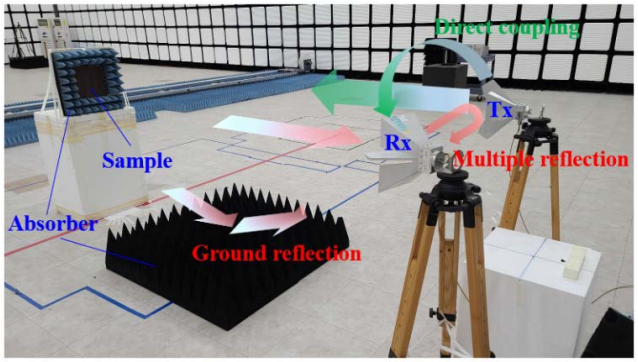

FIGURE 11. Setup for measurements using the fabricated PC array. The transmitting (Tx) and receiving (Rx) antennas were ultra-wideband single-polarized horn antennas covering a range of 1 to 15 GHz and placed at the far-field region relative to the sample. In this figure, the polarizations of the Tx and Rx are vertical and horizontal, respectively (cross-polarization). Measurements were obtained by changing the angle between the two antennas.

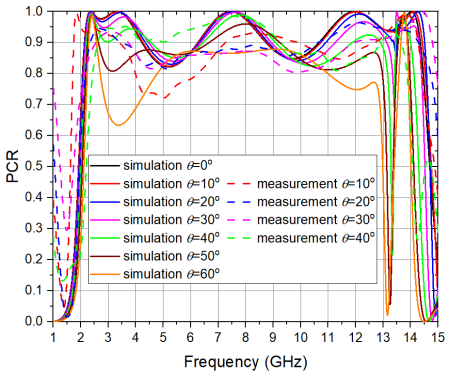

FIGURE 12. Simulated and measured PCRs of the unit cell and fabricated 40 × 40 array structure.

VMSs were attached to the perforated aluminum ground plane, and there were the same number of VMSs as PC elements.

Figure 11 shows the measurement setup for the fabricated PC array based on the NRL arch method [39]. To eliminate the ground reflection signal and edge diffraction of the sample, the absorbers were placed on the plane corresponding to the specular direction of reflection and the edges of the sample. Measurements were obtained by replacing the sample plate with an aluminum plate of the same size for reference reflections. Signals from the sample plate were measured, and the transmission and reception antennas were co-polarized and cross-polarized following the rotation of the Rx antenna by 90°. The measurements were obtained over an angular range of 10° to 40°. The minimum measurement angle was observed due to the physical size of the transmitting and receiving horn antennas, as well as the ambiguity of the multiple reflections between the two antennas and the reflected wave from the sample. The multiple reflections were relatively large when the two antennas were co-polarized. The maximum angle was observed due to the large direct coupling signal that was indistinguishable from the desired reflected signal. To eliminate undesired signals, the time-gated function TG was introduced. Accordingly, r_{xy} and r_{yy} were obtained using Eqs. (1) and (2), respectively:

$$r_{xy} = \left| \frac{TG[S_{21}^{HV}(sample)]}{TG[S_{21}^{VV}(reference)]} \right| \tag{5}$$

$$r_{yy} = \left| \frac{TG[S_{21}^{VV}(sample)]}{TG[S_{21}^{VV}(reference)]} \right| \tag{6}$$

where S_{21} is the transmission coefficient between the transmitting horn antenna port and the receiving horn antenna port, measured by the vector network analyzer (VNA). The first and second letters of the superscripts HV and VV in S_{21} indicate the polarization of the receiving antenna (port 2) and the transmitting antenna (port 1), respectively. H and V refer to the horizontally and vertically polarized antennas, respectively. The terms ''sample'' and ''reference'' in parentheses indicate that the illuminated target is the fabricated PC array or a reference aluminum plate with a same-sized PC array, respectively. Measurements may be obtained sequentially via the inverse fast Fourier transform (IFFT) of the measured frequency domain signal S_{21}, proper time-gating, and a fast Fourier transform (FFT) operation.

The PCR is defined as $|r_{xy}|^2/(|r_{xy}|^2+|r_{yy}|^2)$. In Fig. 12, the measured bandwidth is 1.68 to 14.51 GHz (8.64:1) for PCRs $\geq 72\%$ at an incidence angle of 10°. The corresponding thickness at the lowest operating frequency was 0.08 $\lambda_{1.68\text{GHz}}$. At an incidence angle of 40°, the bandwidth was 2.43 to 13.87 GHz (5.71:1) for PCRs $\geq 80\%$, and the corresponding thickness at the lowest operating frequency was 0.11 $\lambda_{2.35\text{GHz}}$. For a wave incident at an angle of 10° when the transmission and reception antennas are relatively close to each other, the degradation of the measured PCR may result from the imperfect separation of the reflected wave from the sample and the multiple reflected waves between the transmission and reception antennas by the time-gating function. Furthermore, the reception signal at the reception side could be distorted. Although the measured PCR for an incidence angle of 10° at 4 to 6 GHz exhibited degradation, the entire measured operating bandwidth was in good agreement with the simulated bandwidth.

VI. CONCLUSION

In this paper, we presented a novel approach for designing an ultra-broadband and wide-angle-insensitive PC, which can be implemented by simply connecting two orthogonal, tightly coupled dipole arrays in cascade. One TCDA was used as an incident wave reception array antenna, while the other acted as the transmission array antenna in the orthogonal polarization direction. The operation of the proposed PC may be understood considering the equivalent circuit of two orthogonal TCDAs, which is valid according to the reciprocity theorem. We also showed that the TCDA-based PC with a VMS was wide-angle insensitive because the equivalent circuit for the PC corresponded to a cascade connection of

the TCDA in the TE and TM modes. Therefore, the VMS is always effective regardless of the input polarization, which clearly differs from the effect of the VMS in TCDA antennas [22]. It was also found that the ratio of the unit cell size to the height of the PC should be sufficiently small to avoid the common mode generation of oblique incident waves in the band of interest. As a result, for $r_{xy} \geq$ -1 dB, the simulated bandwidth of the unit cell was 2.06 to 14.45 GHz (7.01:1) and 2.19 to 13.89 GHz (6.34:1) at incidence angles of 0° and 50°, respectively. The corresponding thicknesses of the PC were 0.1 $\lambda_{2.06GHz}$ and 0.1 $\lambda_{2.19GHz}$ at the lowest operating frequencies. Compared with other state-of-the-art PCs, the proposed design exhibited an excellent performance and can be used for applications requiring an ultra-wideband and wide-angle-insensitive PC.

REFERENCES

[1] Z. X. Zhang, K. Xu, J. Wu, X. B. Hong, and J. T. Lin, "Two different operation regimes of fiber laser based on nonlinear polarization rotation: Passive mode-locking and multiwavelength emission," *IEEE Photon. Technol. Lett.*, vol. 20, no. 12, pp. 979–981, Jun. 15, 2008.

[2] W. Yang, K. W. Tam, W. W. Choi, W. Che, and H. T. Hui, "Novel polarization rotation technique based on an artificial magnetic conductor and its application in a low-profile circular polarization antenna," *IEEE Trans. Antennas Propag.*, vol. 62, no. 12, pp. 6206–6216, Dec. 2014.

[3] M. Saikia, S. Ghosh, and K. V. Srivastava, "Switchable reflective metamaterial polarisation rotator," *Electron. Lett.*, vol. 52, no. 12, pp. 1030–1032, 2016.

[4] Y. Li, J. Zhang, S. Qu, J. Wang, L. Zheng, A. Zhang, and Z. Xu, "Ultra-broadband linearly polarisation manipulation metamaterial," *Electron. Lett.*, vol. 50, no. 23, pp. 1658–1660, 2014.

[5] S. A. Winkler, W. Hong, M. Bozzi, and K. Wu, "Polarization rotating frequency selective surface based on substrate integrated waveguide technology," *IEEE Trans. Antennas Propag.*, vol. 58, no. 4, pp. 1202–1213, Apr. 2010.

[6] X. Huang, H. Yang, D. Zhang, and Y. Luo, "Ultrathin dual-band metasurface polarization converter," *IEEE Trans. Antennas Propag.*, vol. 67, no. 7, pp. 4636–4641, Jul. 2019.

[7] J. Li, H. Guo, T. Xu, L. Chen, Z. Hang, L. Zhou, and S. Chen, "Multiple-beam interference-enabled broadband metamaterial wave plates," *Phys. Rev. A, Gen. Phys.*, vol. 11, no. 4, Apr. 2019, Art. no. 044042.

[8] H.-X. Xu, S. Sun, S. Tang, S. Ma, Q. He, G.-M. Wang, T. Cai, H.-P. Li, and L. Zhou, "Dynamical control on helicity of electromagnetic waves by tunable metasurfaces," *Sci. Rep.*, vol. 6, no. 1, pp. 1–10, Jun. 2016.

[9] Y.-F. Cheng, X. Ding, W. Shao, and B.-Z. Wang, "Reduction of mutual coupling between patch antennas using a polarization-conversion isolator," *IEEE Antennas Wireless Propag. Lett.*, vol. 16, pp. 1257–1260, 2016.

[10] S. Xiao, S. Yang, H. Zhang, H. Bao, Y. Chen, and S.-W. Qu, "A low-profile wideband tightly coupled dipole array with reduced scattering using polarization conversion metamaterial," *IEEE Trans. Antennas Propag.*, vol. 67, no. 8, pp. 5353–5361, Aug. 2019.

[11] S. Kim and S. Nam, "Extremely low-profile wideband array antenna using TCDA with polarization convertor," *Microw. Opt. Technol. Lett.*, vol. 63, no. 3, pp. 959–964, Mar. 2021.

[12] X. Gao, X. Han, W.-P. Cao, H. O. Li, H. F. Ma, and T. J. Cui, "Ultrawideband and high-efficiency linear polarization converter based on double V-shaped metasurface," *IEEE Trans. Antennas Propag.*, vol. 63, no. 8, pp. 3522–3530, Aug. 2015.

[13] M. Borgese, F. Costa, S. Genovesi, A. Monorchio, and G. Manara, "Optimal design of miniaturized reflecting metasurfaces for ultra-wideband and angularly stable polarization conversion," *Sci. Rep.*, vol. 8, no. 1, pp. 1–11, Dec. 2018.

[14] M. Saikia, S. Ghosh, and K. V. Srivastava, "Design and analysis of ultrathin polarization rotating frequency selective surface using V-shaped slots," *IEEE Antennas Wireless Propag. Lett.*, vol. 16, pp. 2022–2025, 2017.

[15] A. A. Omar, W. Hong, A. Al-Awamry, and A.-E. Mahmoud, "A single-layer vialess wideband reflective polarization rotator utilizing perforated holes," *IEEE Antennas Wireless Propag. Lett.*, vol. 19, no. 12, pp. 2053–2056, Dec. 2020.

[16] M. Karamirad, C. Ghobadi, and J. Nourinia, "Metasurfaces for wideband and efficient polarization rotation," *IEEE Trans. Antennas Propag.*, vol. 69, no. 3, pp. 1799–1804, Mar. 2021.

[17] J. L. Volakis and K. Sertel, "Narrowband and wideband metamaterial antennas based on degenerate band edge and magnetic photonic crystals," *Proc. IEEE*, vol. 99, no. 10, pp. 1732–1745, Oct. 2011.

[18] W. F. Moulder, K. Sertel, and J. L. Volakis, "Superstrate-enhanced ultrawideband tightly coupled array with resistive FSS," *IEEE Trans. Antennas Propag.*, vol. 60, no. 9, pp. 4166–4172, Sep. 2012.

[19] J. P. Doane, K. Sertel, and J. L. Volakis, "A wideband, wide scanning tightly coupled dipole array with integrated balun (TCDA-IB)," *IEEE Trans. Antennas Propag.*, vol. 61, no. 9, pp. 4538–4548, Sep. 2013.

[20] E. Yetisir, N. Ghalichechian, and J. L. Volakis, "Ultrawideband array with 70° scanning using FSS superstrate," *IEEE Trans. Antennas Propag.*, vol. 64, no. 10, pp. 4256–4265, Oct. 2016.

[21] B. Riviere, H. Jeuland, and S. Bolioli, "New equivalent circuit model for a broadband optimization of dipole arrays," *IEEE Antennas Wireless Propag. Lett.*, vol. 13, pp. 1300–1304, 2014.

[22] S. Kim and S. Nam, "Bandwidth extension of dual-polarized 1-D TCDA antenna using VMS," *IEEE Trans. Antennas Propag.*, vol. 67, no. 8, pp. 5305–5312, Aug. 2019.

[23] S. Kim and S. Nam, "A compact and wideband linear array antenna with low mutual coupling," *IEEE Trans. Antennas Propag.*, vol. 67, no. 8, pp. 5695–5699, Aug. 2019.

[24] A. O. Bah, P.-Y. Qin, R. W. Ziolkowski, Y. J. Guo, and T. S. Bird, "A wideband low-profile tightly coupled antenna array with a very high figure of merit," *IEEE Trans. Antennas Propag.*, vol. 67, no. 4, pp. 2332–2343, Apr. 2019.

[25] S. Kim and S. Nam, "Compact ultrawideband antenna on folded ground plane," *IEEE Trans. Antennas Propag.*, vol. 68, no. 10, pp. 7179–7183, Oct. 2020.

[26] S. Kim and S. Nam, "Characteristics of TCDA with polarization converting ground plane," *IEEE Trans. Antennas Propag.*, vol. 69, no. 4, pp. 2359–2364, Apr. 2021.

[27] A. D. Johnson, J. Zhong, S. B. Venkatakrishnan, E. A. Alwan, and J. L. Volakis, "Phased array with low-angle scanning and 46:1 bandwidth," *IEEE Trans. Antennas Propag.*, vol. 68, no. 12, pp. 7833–7841, Jun. 2020.

[28] Q. Luo, S. Gao, W. Li, X. Yang, and G. Wen, "Ultra-wideband and multiband reflectarrays for intelligent multi-functional platforms," in *Proc. 13th Eur. Conf. Antennas Propag.*, 2019, pp. 1–5.

[29] J. Zhang, L. Zhang, Y. Sun, Y. He, and S.-W. Wong, "A broadband single-layer reflectarray antenna based on tightly coupled dipole," in *Proc. IEEE Int. Symp. Antennas Propag.*, Oct. 2019, pp. 1–3.

[30] Y.-M. Cai, W. Li, K. Li, S. Gao, Y. Yin, L. Zhao, and W. Hu, "A novel ultrawideband transmitarray design using tightly coupled dipole elements," *IEEE Trans. Antennas Propag.*, vol. 67, no. 1, pp. 242–250, Jan. 2019.

[31] C. Wu, S. Lu, Z. Yang, and Y. Yashchyshyn, "A UWB absorber based on the TCA concept in the UHF band," *IEEE Trans. Antennas Propag.*, vol. 68, no. 5, pp. 4132–4136, May 2020.

[32] S. Kim and S. Nam, "Ultra-wideband and wide-angle insensitive absorber based on TCDA-under-tightly coupled dipole array," *IEEE Trans. Antennas Propag.*, vol. 69, no. 9, pp. 5682–5690, Sep. 2021.

[33] P. A. Belov, R. Marqués, S. I. Maslovski, I. S. Nefedov, M. Silveirinha, C. R. Simovski, and S. A. Tretyakov, "Strong spatial dispersion in wire media in the very large wavelength limit," *Phys. Rev. B, Condens. Matter*, vol. 67, no. 11, Mar. 2003, Art. no. 113103.

[34] S. Chilukuri and S. Gundappagari, "A wide dual-band metamaterial-loaded antenna for wireless applications," *J. Electromagn. Eng. Sci.*, vol. 20, no. 1, pp. 23–30, Jan. 2020.

[35] D. K. Kong, J. Kim, D. Woo, and Y. J. Yoon, "Broadband modified proximity coupled patch antenna with cavity-backed configuration," *J. Electromagn. Eng. Sci.*, vol. 21, no. 1, pp. 8–14, Jan. 2021.
[36] D. M. Pozar, *Microwave Engineering*, 4th ed. Hoboken, NJ, USA: Wiley, 2011, ch. 12.
[37] R. M. Fano, "Theoretical limitations on the broadband matching of arbitrary impedances," *J. Franklin Inst.*, vol. 249, no. 1, pp. 57–83, Jan. 1950.
[38] J. P. Doane, K. Sertel, and J. L. Volakis, "Matching bandwidth limits for arrays backed by a conducting ground plane," *IEEE Trans. Antennas Propag.*, vol. 61, no. 5, pp. 2511–2518, May 2013.
[39] R. S. Biscaro, E. L. Nohara, and G. G. Peixoto, in *Proc. Int. Microw. Optoelectron. Conf.*, vol. 1, 2003, p. 355.

SEONGJUNG KIM (Student Member, IEEE) received the B.S. degree in electronic and electrical engineering from Hongik University, Seoul, South Korea, in 2017. He is currently pursuing the integrated master's and Ph.D. degree with the Department of Electrical Engineering and Computer Science, Seoul National University, Seoul. His main research interests include metamaterial-based antennas and phased array antennas.

SANGWOOK NAM (Senior Member, IEEE) received the B.S. degree from Seoul National University, Seoul, South Korea, in 1981, the M.S. degree from the Korea Advanced Institute of Science and Technology (KAIST), Seoul, in 1983, and the Ph.D. degree from the University of Texas at Austin, Austin, TX, USA, in 1989, all in electrical engineering. From 1983 to 1986, he was a Researcher at the Gold Star Central Research Laboratory, Seoul. Since 1990, he has been a Professor with the School of Electrical Engineering and Computer Science, Seoul National University. His research interests include the analysis/design of electromagnetic structures, antennas, and microwave active/passive circuits.